VIROLOGY

IFN-λ derived from nonsusceptible enterocytes acts on tuft cells to limit persistent norovirus

Harshad Ingle[1]†, Heyde Makimaa[1]†, Somya Aggarwal[1], Hongju Deng[1], Lynne Foster[1], Yuhao Li[1], Elizabeth A. Kennedy[1], Stefan T. Peterson[1], Craig B. Wilen[2], Sanghyun Lee[3], Mehul S. Suthar[4], Megan T. Baldridge[1,5]*

Norovirus is a leading cause of epidemic viral gastroenteritis, with no currently approved vaccines or antivirals. Murine norovirus (MNoV) is a well-characterized model of norovirus pathogenesis in vivo, and persistent strains exhibit lifelong intestinal infection. Interferon-λ (IFN-λ) is a potent antiviral that rapidly cures MNoV. We previously demonstrated that IFN-λ signaling in intestinal epithelial cells (IECs) controls persistent MNoV, and here demonstrate that IFN-λ acts on tuft cells, the exclusive site of MNoV persistence, to limit infection. While interrogating the source of IFN-λ to regulate MNoV, we confirmed that MDA5-MAVS signaling, required for IFN-λ induction to MNoV in vitro, controls persistent MNoV in vivo. We demonstrate that MAVS in IECs and not immune cells controls MNoV. MAVS in nonsusceptible enterocytes, but not in tuft cells, restricts MNoV, implicating noninfected cells as the IFN-λ source. Our findings indicate that host sensing of MNoV is distinct from cellular tropism, suggesting intercellular communication between IECs for antiviral signaling induction in uninfected bystander cells.

INTRODUCTION

Noroviruses (NoVs) are positive-sense RNA viruses in the *Caliciviridae* family and are the leading cause of nonbacterial gastroenteritis, causing up to 200,000 deaths annually (*1*–*3*). Recent advances in culturing techniques for human NoVs, leveraging human intestinal enteroids (*4*), have revealed that these viruses have a tropism for intestinal epithelial cells (IECs) and are sensitive to regulation by antiviral cytokines interferons (IFNs) (*5*). This IEC tropism is supported by identification of human NoV-infected IECs in intestinal specimens from immunocompromised patients (*6*, *7*). However, the innate immune responses to NoV infections in vivo remain poorly understood.

Over the last two decades, murine norovirus (MNoV) has emerged as a powerful small animal model to study NoV pathogenesis in vivo, and both acute and persistent strains of MNoV have been reported (*8*, *9*). On the basis of cell type–specific expression of the viral receptor CD300LF, persistent MNoV has been found to have a specific and exclusive cellular tropism for tuft cells (*10*–*13*), enigmatic IECs that are important for type II immune responses against parasites (*14*–*16*). Understanding of the tuft cell–specific roles for induction of and response to innate antiviral immune responses, however, is only now beginning to emerge (*13*).

We previously identified IFN-λ as a potent antiviral cytokine in the intestine, with both exogenous and endogenous IFN-λ serving to regulate persistent MNoV infection via signaling through the IFN-λ receptor IFNLR1 on IECs (*17*, *18*). We also previously showed that the transcription factor signal transducer and activator of transcription 1 (STAT1), which controls IFN-stimulated gene (ISG) expression, is required in tuft cells for exogenous IFN-λ to clear persistent MNoV infection (*13*). However, the source of IFN-λ in response to MNoV infection has proven elusive, as expression or localization of cytokine transcripts or protein, either under homeostatic conditions or after infection, is difficult to detect (*18*, *19*). Previous studies have implicated melanoma differentiation–associated protein 5 (MDA5/IFIH1) and adaptor mitochondrial antiviral signaling protein (MAVS; also known as VISA, IPS-1, and CARDIF) in sensing of viral RNA replication products in dendritic cells (DCs) to induce type I and III IFN responses to acute and persistent MNoV strains (*20*, *21*). MAVS has also been implicated in sensing of human NoV in human intestinal enteroids (*5*).

Here, we confirmed that MAVS and MDA5 are required for control of persistent MNoV in vivo, and further leveraged mice conditionally deficient for either *Ifnlr1* or *Mavs* to delineate the cell-specific requirements for these genes in both the response to and induction of IFN-λ. While *Ifnlr1* expression by tuft cells is required for the antiviral activity of IFN-λ, surprisingly we found that tuft cells are not implicated as the source of IFN-λ, with enterocytes instead responsible for MAVS-mediated IFN responses to MNoV infection. These findings indicate that intercellular cross-talk among IECs, driven by viral sensing by nonsusceptible enterocytes and mediated through IFN-λ signaling on permissive tuft cells, is a critical aspect of the intestinal innate immune response to MNoV infection.

RESULTS

IFN-λ is derived from radiation-insensitive cells for control of persistent MNoV

Previous studies have identified short-lived tuft cells as the reservoir for persistent MNoV strain CR6 (*12*, *13*) and revealed intact IFN-λ signaling as critical to limiting the number of infected tuft cells (*22*).

[1]Division of Infectious Diseases, Department of Medicine, Edison Family Center for Genome Sciences & Systems Biology, Washington University School of Medicine, St. Louis, MO, USA. [2]Departments of Laboratory Medicine and Immunobiology, Yale School of Medicine, New Haven, CT, USA. [3]Division of Biology and Medicine, Department of Molecular Microbiology and Immunology, Brown University, Providence, RI, USA. [4]Department of Pediatrics, Emory School of Medicine, Atlanta, GA, USA. [5]Department of Molecular Microbiology, Washington University School of Medicine, St. Louis, MO, USA.
*Corresponding author. Email: mbaldridge@wustl.edu
†These authors contributed equally to this work.

While IFN-λ signaling in the intestinal epithelium is thus critical to the control of MNoV persistence, the cellular source of IFN-λ after CR6 infection is unknown. Our previous work has suggested the possibility of immune cells, such as DCs, as a source of intestinal IFN-λ both under homeostatic conditions and in response to MNoV (*19*, *21*). We recently described *Ifnl2*$^{-/-}$*Ifnl3*$^{-/-}$ mice, which are incapable of producing IFN-λ and phenocopy *Ifnlr1* deficiency (*23*). We generated reciprocal bone marrow chimeras using wild-type (WT) and *Ifnl2*$^{-/-}$*Ifnl3*$^{-/-}$ donors and recipients and then infected them with CR6. IFN-λ derived from radiation-insensitive cells, as opposed to radiation-sensitive hematopoietic cells, was required to control CR6 levels in both stool and tissues (Fig. 1, A and B), indirectly suggesting that the intestinal epithelium could be a potential source of IFN-λ to regulate persistent MNoV.

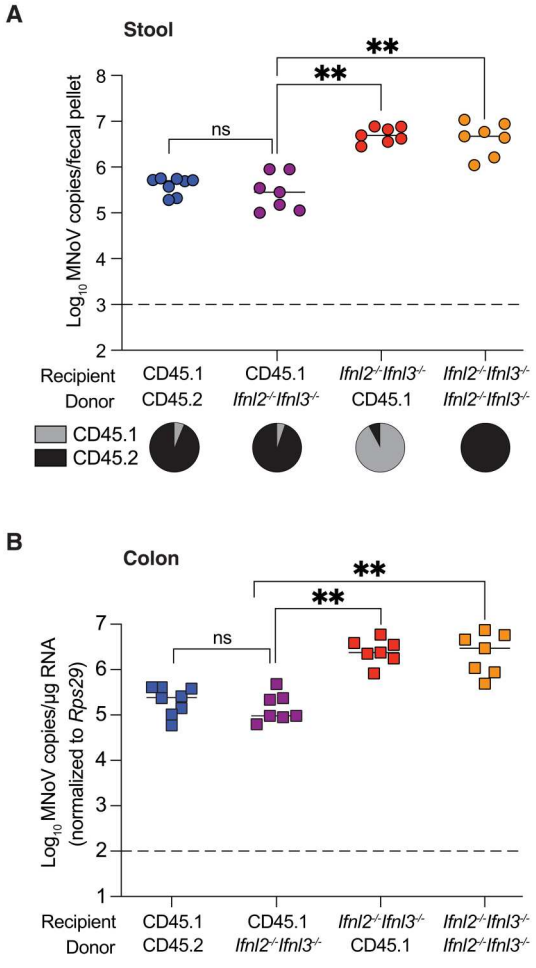

Fig. 1. IFN-λ is derived from radiation-insensitive cells for control of persistent MNoV. (**A** and **B**) MNoV genome copies in fecal pellets (A) and colon (B) at 7dpi with CR6 in bone marrow chimeras (n = 7 to 8) generated from WT and *Ifnl2*$^{-/-}$*Ifnl3*$^{-/-}$ mice as indicated. Pie chart depicting percentage of chimerism in peripheral blood at 8 weeks after transplant before MNoV infection. Results were analyzed using Kruskal-Wallis analysis of variance (ANOVA) with Dunn's post-test from two independent experiments. $^{**}P < 0.01$; ns, not significant. Bars indicate mean of all data points.

MDA5-MAVS signaling controls persistent MNoV infection in vivo

To further define the source of IFN-λ for regulation of CR6, we first elected to confirm signals upstream of IFN-λ that are critical for its production. While it has been reported that MDA5-MAVS signaling is required for IFN-λ induction in bone marrow DCs after CR6 infection in vitro (*21*), regulation of CR6 by this pathway has not been assessed in vivo. We infected *Mavs*$^{-/-}$ mice and found elevated CR6 levels in both stool and intestinal tissue samples at 7 days post-infection (dpi) compared to controls (Fig. 2, A and B). Similarly, CR6 infection of *Mda5*$^{-/-}$ mice was associated with increased viral levels in stool and tissue with a concomitant increase in infected tuft cells (Fig. 2, C and D). In addition, consistent with what has been previously reported in *Ifnlr1*$^{-/-}$ mice (*22*), we found a higher number of CR6-positive tuft cells in *Mavs*$^{-/-}$ and *Mda5*$^{-/-}$ mice despite an equivalent total number of tuft cells, indicating a defect in viral control in the absence of MAVS signaling (Fig. 2, E and F). Together, these findings support that CR6 infection is regulated by MDA5-MAVS–mediated induction of IFN-λ in vivo.

MAVS is required in IECs for control of persistent MNoV

Because persistent MNoV infects IECs (*12*, *22*), but has been shown to induce MAVS-dependent IFN-λ responses in DCs (*21*), we elected to explore how MAVS in DCs and IECs regulates CR6 using mice conditionally deficient for *Mavs* (*24*). To this end, we generated *Mavs*$^{f/f}$*-Cd11ccre* and *Mavs*$^{f/f}$*-Vilcre* mice, respectively, crossed to DC-specific CD11c-Cre (*25*) and IEC-specific Villin-Cre (*26*). Upon infection with CR6, we found no difference in viral levels in *Mavs*$^{f/f}$*-Cd11ccre* mice compared to littermate controls (fig. S1), consistent with our results indicating the source of IFN-λ to be radiation-insensitive nonhematopoietic cells (Fig. 1, A and B). In contrast, upon CR6 infection of *Mavs*$^{f/f}$*-Vilcre* mice, in which *Mavs* expression is depleted in IECs (Fig. 3A), we observed higher viral levels in stool and tissue, phenocopying our findings in *Mavs*$^{-/-}$ mice (Fig. 3, B and C). These data indicate that MAVS in IECs is necessary to limit in vivo CR6, further supporting that virus-induced IFN-λ is IEC-derived.

MAVS in tuft cells is dispensable for control of persistent MNoV

As the cellular tropism of persistent MNoV is restricted to tuft cells (*10*, *12*, *13*), we speculated that MAVS-dependent signaling in tuft cells could be critical for regulating CR6 infection. To test this, we generated *Mavs*$^{f/f}$*-Dclk1cre* mice in which *Mavs* expression is depleted specifically in tuft cells (Fig. 3D). *Mavs*$^{f/f}$*-Dclk1cre* mice did not show any difference in CR6 levels compared to *Mavs*$^{f/f}$ littermates (Fig. 3, E and F), suggesting that tuft cells are unlikely to be the predominant source of IFN-λ to restrict CR6.

To confirm this unexpected finding, we sought to identify another Cre line active in tuft cells. Previously, single-cell RNA sequencing (RNAseq) analysis identified two distinct subsets of intestinal tuft cells designated as Tuft-1 and Tuft-2 (*27*). While Tuft-1 cells express markers for neuronal development, Tuft-2 cells express immune-related genes. MNoV receptor *Cd300lf* is expressed exclusively in tuft cells (detected in ~20.5% of tuft cells), and in particular in Tuft-2 cells (fig. S2, A and B) (*27*). Because *Vav1*, in addition to being expressed in hematopoietic cells, is also expressed specifically only in tuft cells (detected in ~57.2% of tuft cells) with higher expression in Tuft-2 cells (*27*) (fig. S2, A and

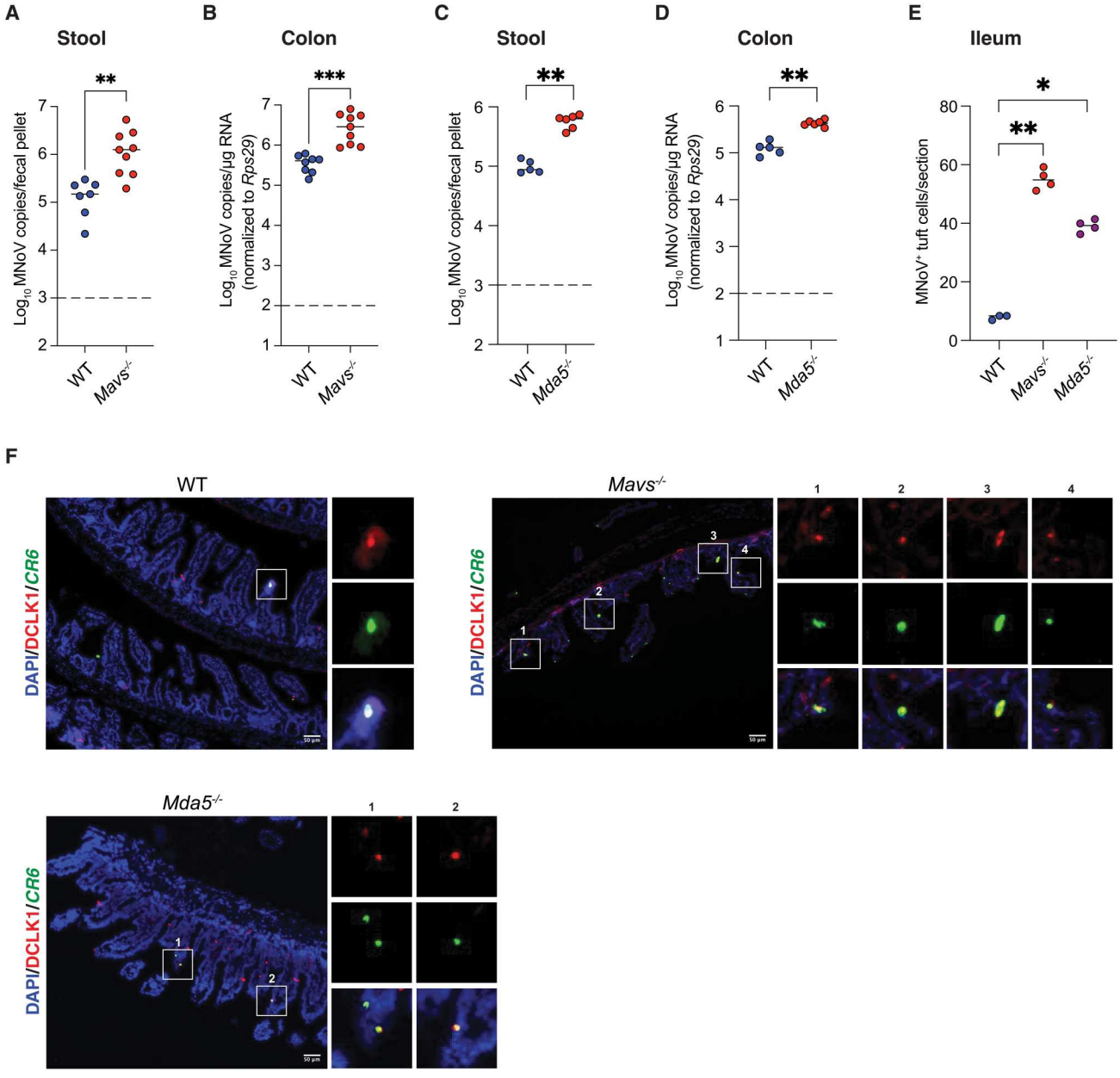

Fig. 2. *Mavs/Mda5* axis is critical for controlling persistent MNoV infection. (**A** to **D**) MNoV genome copies in fecal pellets and colon tissues of WT ($n = 5$ to 7), *Mavs*$^{-/-}$ ($n = 9$), and *Mda5*$^{-/-}$ ($n = 6$) mice at 7 dpi. (**E**) Quantification of CR6-positive tuft cells per tissue section of the entire ileum, with portions of ileum sections depicted in (F). (**F**) Representative ileal sections of WT, *Mavs*$^{-/-}$, and *Mda5*$^{-/-}$ mice at 7 dpi with CR6, hybridized with probes for MNoV (green) and stained with anti-DCLK1 (red). Cell nuclei were stained using DAPI (blue). Results were analyzed by Mann-Whitney test (A to D) from three (A and B) and two (C to E) independent experiments. $^{**}P < 0.01$; $^{*}P < 0.05$. Bars indicate mean of all data points. White boxes reflect the magnified inset images.

C), we anticipated that Vav-iCre should also be active in MNoV-susceptible tuft cells. We generated *R26-stop-EYFP-VaviCre* mice, in which EYFP is expressed in cells expressing *Vav*. We confirmed EYFP expression, and therefore Vav-iCre activity, in ~10% of cells positive for SiglecF, a marker for tuft cells (fig. S2D) (*28*). We then crossed *Mavs*$^{f/f}$ mice to *Vav-iCre* to disrupt *Mavs* in both hematopoietic cells and tuft cells, confirming depletion of *Mavs* expression in splenocytes and in sorted tuft cells from *Mavs*$^{f/f}$*-VaviCre* mice (Fig. 3, G and H). The modest depletion of *Mavs* in *Mavs*$^{f/f}$*-VaviCre* tuft cells may reflect the heterogeneous *Vav1* expression in this cell type (fig. S2, C and D). Similar to our results in *Mavs*$^{f/f}$*-Dclk1cre* mice, CR6 levels in *Mavs*$^{f/f}$*-VaviCre* mice were equivalent to *Mavs*$^{f/f}$ controls (Fig. 3, I and J), thereby confirming that MAVS-associated sensing of CR6 in tuft cells is not required for control of infection. Thus, while the tropism of CR6 is restricted to tuft cells, innate immune sensing of CR6 appears to occur in other IEC types.

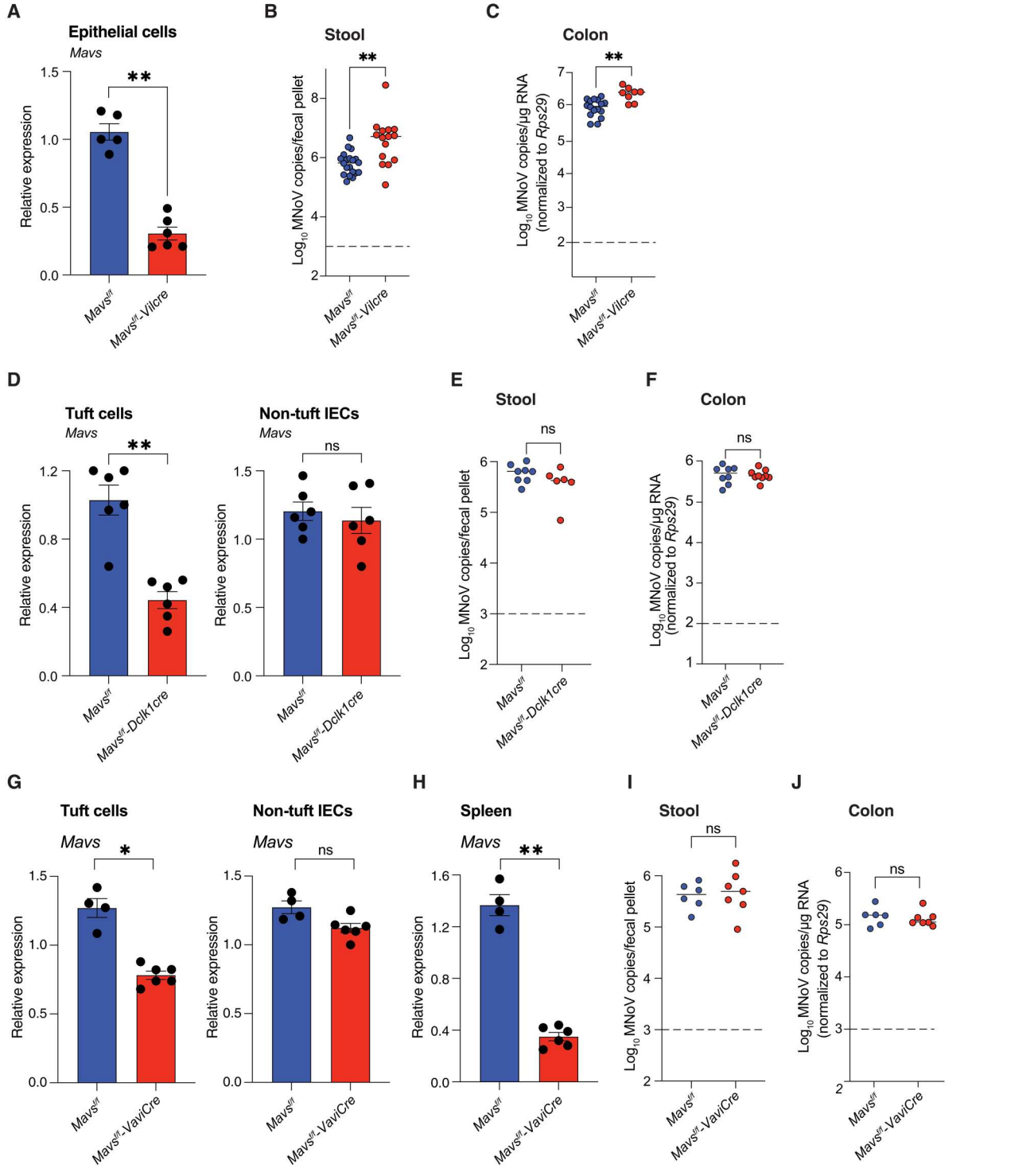

Fig. 3. *Mavs* is required in epithelial cells but is dispensable in tuft cells for control of persistent MNoV. (**A**) Relative quantification of *Mavs* mRNA levels in IECs from small intestine of *Mavs*$^{f/f}$ ($n = 5$) and *Mavs*$^{f/f}$*-Vilcre* ($n = 5$) mice. (**B** and **C**) MNoV genome copies in fecal pellets and colon tissues of *Mavs*$^{f/f}$ ($n = 18$) and *Mavs*$^{f/f}$*-Vilcre* ($n = 15$) mice at 7 dpi with CR6. (**D**) Relative quantification of *Mavs* mRNA levels in tuft cells from small intestine of *Mavs*$^{f/f}$ ($n = 6$) *and Mavs*$^{f/f}$*-Dclk1cre* ($n = 6$) mice. (**E** and **F**) MNoV genome copies in fecal pellets and colon tissues of *Mavs*$^{f/f}$ ($n = 8$) and *Mavs*$^{f/f}$*-Dclk1cre* ($n = 8$) mice at 7 dpi with CR6. (**G** and **H**) Relative quantification of *Mavs* mRNA levels in (G) tuft cells and nontuft IECs, and (H) splenocytes from small intestine of *Mavs*$^{f/f}$ ($n = 4$) and *Mavs*$^{f/f}$*-Vavicre* ($n = 6$) mice. (**I** and **J**) MNoV genome copies in fecal pellets and colon tissues of *Mavs*$^{f/f}$ ($n = 6$) and *Mavs*$^{f/f}$*-VaviCre* ($n = 6$) mice at 7 dpi with CR6. Results were analyzed by Mann-Whitney test (A to F, I, and J) from three (A to E) and two (I and J) independent experiments. *$P < 0.05$; **$P < 0.01$. Bars indicate mean of all data points.

MAVS in enterocytes, and not secretory cells, is critical for control of persistent MNoV

We evaluated *Mavs* expression across IEC types and found that it was detected in similar proportions of cells across all IEC clusters (between 4.2 and 13.6% of cells) (*27*) (fig. S2, A and E), precluding identification of other obvious candidate IEC types. Thus, to delineate the specific subset of IECs responsible for virus sensing and IFN regulation, we next crossed $Mavs^{f/f}$ mice to *Math1cre* (*29*) and $Alpicre^{ERT2}$ (*30*) lines for targeted depletion of *Mavs* in secretory cells, including goblet, Paneth, enteroendocrine, and tuft cells (*31*, *32*), or enterocytes, respectively. We confirmed that *Mavs* was depleted in sorted goblet cells, but not IECs in general, of $Mavs^{f/f}$-*Math1cre* mice (Fig. 4A), but found no effect of disrupted *Mavs* in secretory cells for CR6 levels in stool or tissue (Fig. 4, B and C). In contrast, when we induced disruption of *Mavs* in enterocytes by treating $Mavs^{f/f}$-$Alpicre^{ERT2}$ mice with tamoxifen (Fig. 4D), we observed a statistically significant increase in CR6 levels in stool, colon, and ileum compared to tamoxifen-treated $Mavs^{f/f}$ controls (Fig. 4, E to G), implicating enterocytes as the cell type responsible for sensing of viral infection and IFN production. We confirmed that in $Mavs^{f/f}$-$Alpicre^{ERT2}$ mice, CR6 exhibited an expanded tropism for tuft cells (Fig. 4, G and H).

While it is known that *Ifnlr1* expression by IECs is critical for regulation of persistent MNoV (*17*), with the surprising observation of enterocytes as important for CR6 sensing, we sought to confirm that IFN-λ signaling was not also acting on enterocytes. We assessed CR6 levels in tamoxifen-treated $Ifnlr1^{f/f}$-$Alpicre^{ERT2}$ mice and found that they were comparable to $Ifnlr1^{f/f}$ mice, confirming that IFN-λ signaling in enterocytes is dispensable for regulation of persistent MNoV infection (fig. S3).

IFN-λ acts on tuft cells to control persistent MNoV infection in vivo

In WT mice, only ~1.4% of tuft cells and between 0.002 and 0.01% of total colonic IECs are infected by CR6 (*12*, *22*), a proportion that is increased ~3-fold in $Ifnlr1^{-/-}$ mice (*22*). Perhaps unsurprisingly considering the rarity of infected cells in the intestine, previous efforts to visualize infected tuft cells by transmission electron microscopy (TEM) in WT mice infected with CR6 have been unsuccessful. We leveraged the expanded viral tropism of CR6 in the absence of IFN-λ signaling, as well as the tuft cell hyperplasia induced by succinate treatment (*28*), to enhance our likelihood of identifying a CR6-infected tuft cell by TEM in succinate-treated $Ifnlr1^{-/-}$ intestines at 7 dpi. We confirmed enhanced CR6 levels in these mice (Fig. 5A and fig. S4, A and B) and observed rare tuft cells containing microvesicular bodies encapsulating putative virions (Fig. 5B). We assessed the diameter of these putative virions (36 to 56 nm) and found them to be similar in size and appearance to virions derived from a purified tissue culture stock of CR6 prepared from BV2 cells (41 to 47 nm) (Fig. 5, C and D). Both were larger than the originally reported size of MNV-1 virions (28 to 35 nm) (*33*), a distinct MNoV strain. These images represent the first potential electron microscopy (EM) imaging of NoV-infected IECs in vivo and serve to support our established understanding of tuft cells as the exclusive site of CR6 infection.

While a requirement for STAT1 in tuft cells to regulate MNoV infection has been established (*13*), we sought to definitively assess whether IFN-λ acts directly on tuft cells to limit CR6 infection. We first treated ISG reporter $Mx1^{gfp}$ mice (*34*), which exhibit green fluorescent protein (GFP) fluorescence in response to IFN signaling, with exogenous IFN-λ to determine whether tuft cells were capable of responding to IFN-λ signaling with ISG expression. We detected GFP-positive tuft cells among numerous GFP-positive IECs in the ileum (Fig. 5E), supporting that tuft cells can respond to IFN-λ similarly to other IECs. We next generated $Ifnlr1^{f/f}$-*Dclk1cre* mice in which *Ifnlr1* expression is specifically depleted in tuft cells (Fig. 5F). Abrogation of IFN-λ signaling in tuft cells resulted in enhanced shedding of CR6 in the stool (Fig. 5G), higher colonic viral levels at 7 dpi (Fig. 5H), and an expansion of infected tuft cells (fig. S4, C and D) similar to what we have reported when *Ifnlr1* expression is depleted in all IECs (*22*) and to what we observed in the context of disruption of *Mda5* or *Mavs* (Fig. 2, E and F). Additionally, $Ifnlr1^{f/f}$-*Dclk1cre* mice treated with exogenous IFN-λ failed to clear persistent CR6 infection, although robust clearance was observed in $Ifnlr1^{f/f}$ littermates consistent with previous reports (*17*, *18*) (Fig. 5, G and H). Our results demonstrate that intestinal tuft cells directly respond to IFN-λ to restrict MNoV persistence. In sum, our data indicate that nonsusceptible enterocytes are critical for sensing viral infection and mounting the key innate immune response against persistent MNoV to limit expanded infection of permissive cells.

DISCUSSION

Here, we investigated the activity and source of IFN-λ during persistent MNoV infection in intestinal tuft cells. Intestinal tuft cell turnover generates short-lived tuft cells with a life span of at least 7 days and long-lived tuft cells that survive up to 18 months (*32*, *35*–*37*). Short-lived intestinal tuft cells act as a bona fide reservoir for CR6 in vivo (*10*, *12*, *13*). However, the extreme rarity of infected tuft cells has made it challenging to structurally evaluate MNoV-infected tuft cells, a barrier we overcame by removing IFN-λ signaling and enhancing tuft cell numbers with succinate treatment to substantially enhance the number of infected cells. Several enteric viruses including rotavirus, human NoV, and the MNV-1 strain of MNoV have been reported to be shed in microvesicular bodies (*38*). For the first time, we report that MNoV-infected tuft cells contain microvesicular bodies with multiple putative virions present. These putative CR6 virions we detected in tuft cells are similar in size to CR6 virions isolated from BV2 cells, both of which are larger than the previously reported MNV-1 virion size (*33*). They share a similar size with $T = 3$ and $T = 4$ icosahedral human NoV GII.4c virus-like particles (46 and 50 nm, respectively) (*39*). While numerous studies have characterized the capsid structure for MNV-1 (*40*–*42*), structural studies for CR6 are lacking. Recent reports have shown that the capsid of MNV-1 can be highly dynamic and influenced by binding of cofactors such as bile acids that augment binding of MNV-1 capsid to its cognate receptor (*40*, *41*, *43*). The relative plasticity and context dependence of the CR6 capsid conformation remains an important area for future study.

We previously established that IFN-λ signaling in IECs is required to control CR6 in vivo (*17*), and STAT1 in tuft cells is critical for the antiviral activity of exogenous IFN-λ to limit CR6 (*13*). Here, we confirmed and extended these findings by demonstrating that tuft cells can sense and respond to IFN-λ to induce ISGs, and that IFNLR1 expression on tuft cells, and not enterocytes, is critical for the antiviral activity of endogenous and exogenous IFN-λ.

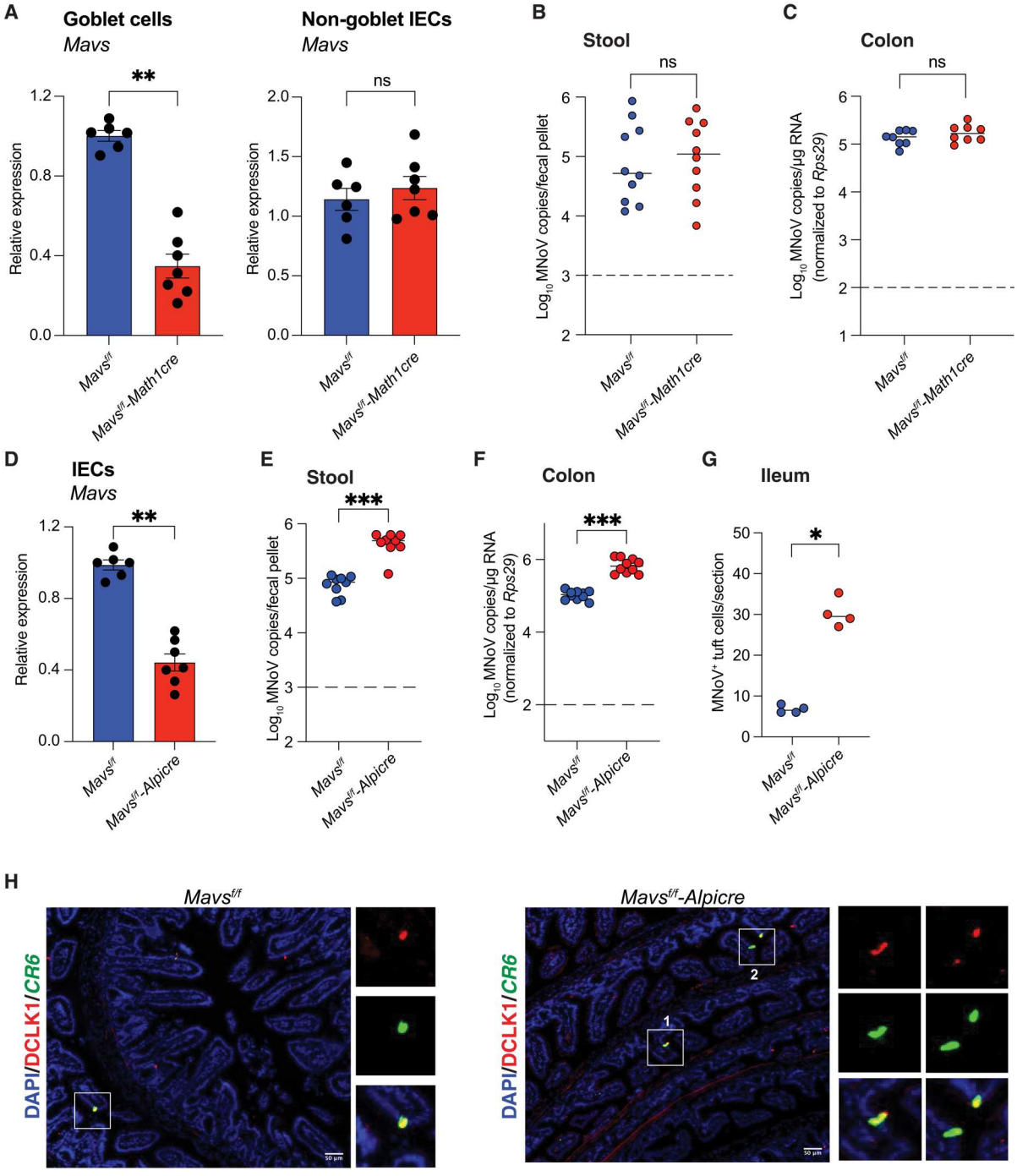

Fig. 4. *Mavs* is dispensable in secretory cells but required in enterocytes for control of persistent MNoV. (**A**) Relative quantification of *Mavs* mRNA levels in goblet cells and nongoblet IECs from small intestine of *Mavs*$^{f/f}$ ($n = 6$) and *Mavs*$^{f/f}$-*Math1cre* ($n = 7$) mice. (**B** and **C**) MNoV genome copies in fecal pellets and colon tissues of *Mavs*$^{f/f}$ ($n = 10$) and *Mavs*$^{f/f}$-*Math1cre* ($n = 7$ to 10) mice at 7 dpi with CR6. (**D**) Relative quantification of *Mavs* mRNA levels in IECs from *Mavs*$^{f/f}$ and *Mavs*$^{f/f}$-*Alpicre*^{ERT2} at 3 days after tamoxifen treatment. (**E** and **F**) MNoV genome copies in fecal pellets and colon tissues of *Mavs*$^{f/f}$ ($n = 9$) and *Mavs*$^{f/f}$-*Alpicre*^{ERT2} ($n = 10$) mice at 7 dpi. (**G**) Quantification of CR6-positive tuft cells in the entire ileum, with portions of ileum sections depicted in (H). (**H**) Representative ileal sections of WT, *Mavs*$^{-/-}$, and *Mda5*$^{-/-}$ mice at 7 dpi with CR6, hybridized with probes for MNoV (green) and stained with anti-DCLK1 (red). Cell nuclei were stained using DAPI (blue). Results were analyzed by Mann-Whitney test (A to G) from three (A to F) and two (G and H) independent experiments. ***$P < 0.001$; **$P < 0.01$; *$P < 0.05$. Bars indicate mean of all data points. White boxes reflect the magnified inset images.

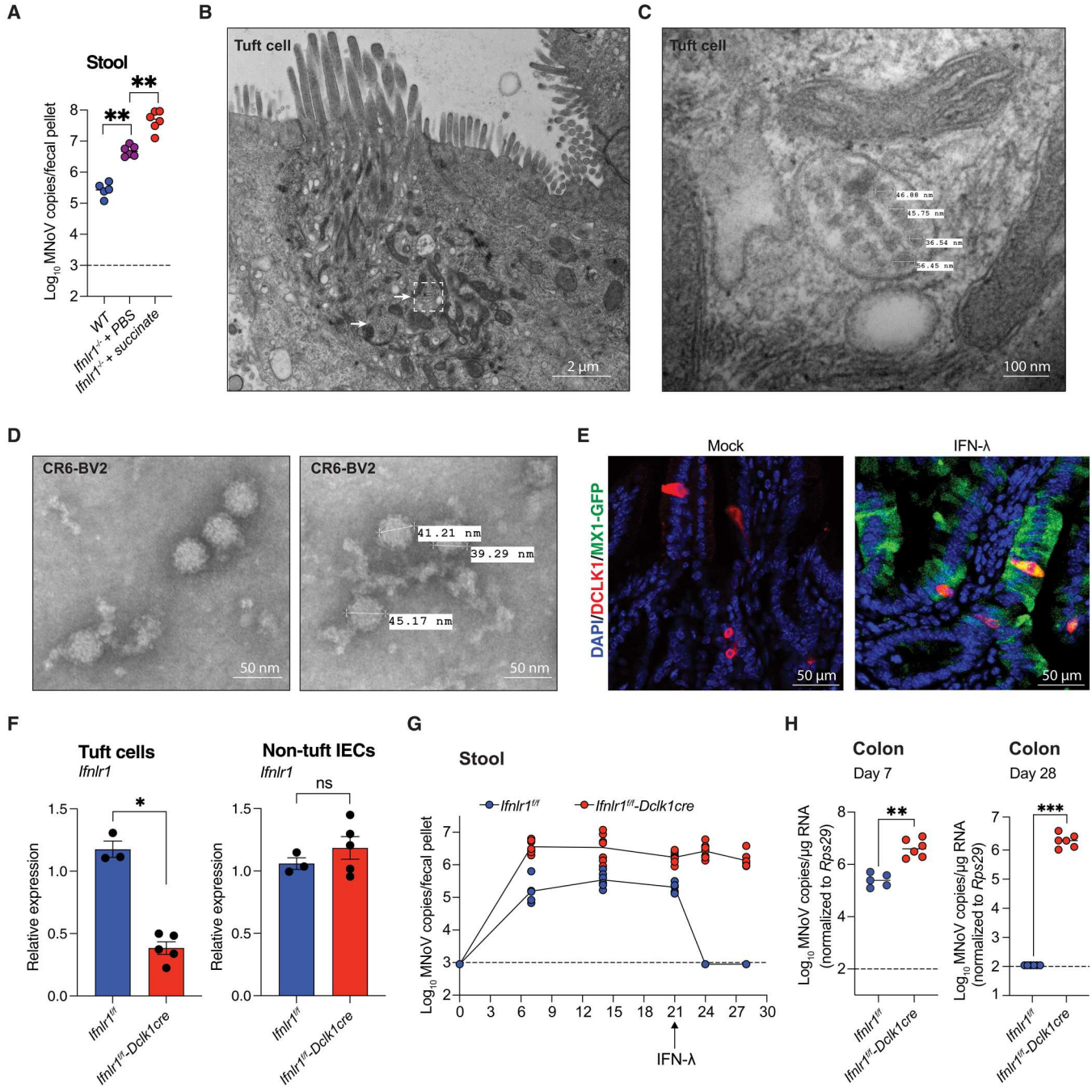

Fig. 5. IFN-λ acts on tuft cells to regulate persistent MNoV infection. (**A**) MNoV genomes quantified in fecal pellets of WT ($n = 5$), *Ifnlr1*$^{-/-}$ treated with PBS ($n = 5$), and *Ifnlr1*$^{-/-}$ mice treated with succinate ($n = 6$) at 7 dpi. (**B**) Electron microscopy (EM) images of tuft cell from CR6-infected *Ifnlr1*$^{-/-}$ mice pretreated with succinate. Microvesicular bodies (MVBs) containing putative MNoV are denoted by arrows, and white box denotes corresponding magnified image in (C). (**C**) Magnified image of MVB depicting putative CR6 virion size. (**D**) EM images of CR6 virions isolated from BV2 cells. (**E**) Immunofluorescence images of ileal sections of *Mx1*^{gfp} mice treated with mock (PBS) or IFN-λ for 24 hours, with tuft cell marker DCLK1 (red) and GFP (green). Cell nuclei were stained using DAPI (blue). (**F**) Relative quantification of *Ifnlr1* mRNA levels in tuft cells and nontuft IECs from small intestine (SI) of *Ifnlr1*$^{f/f}$ ($n = 3$) and *Ifnlr1*$^{f/f}$*-Dclk1cre* ($n = 5$) mice. (**G** and **H**) Longitudinal analysis of MNoV genome copies in fecal pellets of *Ifnlr1*$^{f/f}$ ($n = 6$) and *Ifnlr1*$^{f/f}$*-Dclk1cre* ($n = 7$) mice infected with CR6 for 21 days before IFN-λ treatment, and colon tissues at 28 dpi. Results were analyzed using Kruskal-Wallis ANOVA with Dunn's post-test (A) and Mann-Whitney test (F to H) from two independent experiment. ***$P < 0.001$; **$P < 0.01$; *$P < 0.05$. Bars indicate mean of all data points.

Specifically, we found that IFN-λ signaling in tuft cells limits the number of infected cells, consistent with a previous report (*22*). Thus, the induction of endogenous IFN-λ upon CR6 infection acts broadly on tuft cells throughout the epithelium to prevent infection of most tuft cells, confirming innate immune protection as a key determinant of tuft cell permissiveness to CR6 infection.

While IFN-λ is clearly a critical cytokine for regulation of CR6, the mechanisms associated with IFN-λ induction by CR6 have remained enigmatic, as varied attempts at direct detection of IFN-λ at the transcript or protein level have failed. We thus chose to explore induction using different knockout mouse models. The innate immune sensing pathways contributing to IFN-λ induction after CR6 infection in vivo have not been previously defined, but our previous work demonstrated that MDA5 is important for IFN-λ induction in response to CR6 infection in bone marrow–derived DCs (*21*). MDA5 senses positive-strand RNA viruses, leading to IFN production via MAVS (*20*, *44*). Here, we showed that mice lacking *Mda5* exhibited higher CR6 levels in stool and tissue, phenotypes that are also present in *Mavs*$^{-/-}$ mice. These results, which correlate well with our observations in *Ifnlr1*$^{-/-}$ mice, strongly suggest that the MDA5-MAVS pathway is key for in vivo IFN-λ induction by CR6.

In a previous study, we demonstrated that *Ifnl2*$^{-/-}$*Ifnl3*$^{-/-}$ mice display defective control of MNoV and other mucosal viruses, and therefore recapitulate *Ifnlr1* deficiency (*23*). Bone marrow chimeras generated from *Ifnl2*$^{-/-}$*Ifnl3*$^{-/-}$ and WT mice support that IFN-λ is derived from radiation-insensitive cells. This finding is further bolstered by our observation that CR6 viral levels are unchanged in mice lacking *Mavs* in hematopoietic cells, and that instead IEC-specific deletion of *Mavs* enhances CR6 infection. As tuft cells are the only IEC type permissive to CR6 in vivo, we depleted *Mavs* in tuft cells using several different Cre lines that either specifically target tuft cells (*Dclk1cre-Mavs*$^{f/f}$) or target tuft cells in addition to other cell types (*Mavs*$^{f/f}$*-VaviCre* and *Mavs*$^{f/f}$*-Math1cre*). We observed that mice lacking *Mavs* expression in tuft cells showed no difference in CR6 infection, indicating that although tuft cells are the exclusive permissive cells in the intestine, they are not responsible for sensing and producing IFN-λ to limit CR6 infection. Because our data implicated IECs, but ruled out other secretory cells including Paneth, goblet, and enteroendocrine cells, we assessed mice with enterocyte-specific deletion of *Mavs* and found increased CR6 levels in stool and tissue. Thus, sensing of CR6 by MAVS to drive IFN-λ induction in nonsusceptible enterocytes occurs fully independently of the response to IFN-λ by tuft cells to limit CR6 persistence.

Bystander IEC responses have been previously reported in the context of *Listeria monocytogenes* and *Salmonella typhimurium* infection, wherein activation of nuclear factor κB (NFκB) and mitogen-activated protein (MAP) kinase signaling was propagated from infected to uninfected neighboring cells via gap junctions leading to induction of antibacterial immune responses (*45*). STING activation by cyclic guanosine monophosphate–adenosine monophosphate transfer from producing cells to neighboring cells via gap junctions has also been identified as a putative mechanism of innate immune induction in trans (*46*). A distinctive feature of tuft cells is cytospinules, lateral projections that penetrate neighboring IECs and represent a potential conduit for targeted delivery of cargo (*47*). This raises the intriguing possibility of delivery of viral RNA from tuft cells to neighboring enterocytes for MDA5/MAVS-mediated induction of antiviral IFN responses. Alternatively, a recent study (*48*) identified exosome carriage of coxsackievirus B3 as a means for viral infection of receptor-negative immune cells. All evidence to date indicates that tuft cells are required for productive CR6 infection (*10*, *12*, *13*, *49*), but it is possible that either nonproductive infection of or cell surface interactions with enterocytes could serve as means by which antiviral responses are initiated via luminal virus. Further studies will be required to define the physiological significance of cytospinules, gap junctions, and/or exosomes in controlling tuft cell communication with neighboring enterocytes and to clarify the specific mechanisms by which antiviral immune responses are induced to control CR6 pathogenesis in vivo. Thus, in some scenarios, the classic model of IFNs being induced and derived predominantly from virally infected cells should be replaced by uninfected neighboring cells providing protective intercellular antiviral signaling.

MATERIALS AND METHODS

Mice

Mice of both sexes, aged 6 to 12 weeks, were used in all experiments. Experimental mice were cohoused with up to five mice of the same sex per cage with autoclaved standard chow pellets and water provided ad libitum. Animal protocols were approved by the Washington University Institutional Animal Care and Use Committee (protocol numbers 20160126, 20190162, and 22-1040). WT C57BL/6J (JAX stock #000664; also designated as CD45.2) mice were originally purchased and maintained as a local breeding colony at Washington University School of Medicine under specific pathogen–free conditions according to University guidelines. WT C57BL/6J CD45.1 mice (JAX stock #002014) (*50*) were obtained for bone marrow chimera studies.

Ifnlr1$^{f/f}$ (*Ifnlr1*$^{tm1a(EUCOMM)Wtsi}$) mice (*17*) were crossed to *Dckl1cre* mice (provided by T. Wang) (*37*) for selective constitutive disruption of *Ifnlr1* in tuft cells or *Alpicre*^{ERT2} mice (provided by H. Clevers and O. Yilmaz) (*30*) for selective disruption in enterocytes. Generation of *Ifnlr1*$^{-/-}$ mice was previously described (*17*); briefly, these mice were established by interbreeding *Ifnlr1*$^{tm1a(EUCOMM)Wtsi}$ mice and Deleter-Cre mice, followed by backcrossing by speed congenics onto a C57BL/6J background. *Ifnl2*$^{-/-}$*Ifnl3*$^{-/-}$ mice have been previously described (*23*).

Mavs$^{f/f}$ mice have been previously described (*24*). These were crossed to *Cd11ccre* (DCs and alveolar macrophages) (*25*), *Villincre* (IECs) (*26*), *Vavicre* (hematopoietic and intestinal tuft cells; JAX stock #008610) (*51*), *Dckl1cre* (tuft cells) (*37*), *Math1cre* (secretory IECs; JAX stock #011104) (*29*), and *Alpicre*^{ERT2} (enterocytes) (*30*) lines for selective disruption of *Mavs* in the indicated cell types.

Mx1^{gfp} mice (JAX stock #033219) have been previously described (*34*). *Vavicre* mice (JAX stock #008610) (*51*) were crossed to *R26-stop-EYFP* (JAX stock #006148) (*52*) to generate *R26-stop-EYFP-Vavicre* mice.

Generation of MNoV stocks and determination of titers

Stocks of MNoV strain CR6 were generated from a molecular clone as previously described (*53*). Briefly, a plasmid encoding the CR6 genome was transfected into 293T cells to generate infectious virus, which was subsequently passaged on BV2 cells. After two passages, BV2 cultures were frozen and thawed to liberate virions. Cultures were then cleared of cellular debris, and virus was

concentrated by ultracentrifugation. Titers of virus stocks were determined by plaque assay on BV2 cells (*54*).

Infections and treatments

For MNoV infections, mice were inoculated with a dose of 10^6 plaque-forming units of strain CR6 by the oral route in a volume of 25 μl. Recombinant IFN-λ was provided by Bristol Myers Squibb (Seattle, WA) as a monomeric conjugate composed of 20-kDa linear polyethylene glycol (PEG) attached to the N terminus of murine IFN-λ, as previously reported (*18*). For treatment of mice, 3 μg of IFN-λ diluted in phosphate-buffered saline (PBS) was injected intraperitoneally.

For succinate treatment, mice were administered 150 mM sodium succinate in drinking water for 5 days before inoculation with CR6 and were maintained on succinate until intestinal sections were collected at 7 dpi. For tamoxifen treatment, mice were intraperitoneally injected with tamoxifen (Sigma-Aldrich, USA) or 4-hydroxytamoxifen (Sigma-Aldrich, USA) at 5 mg/kg of body weight 1 day before infection as well as at 2 and 5 dpi.

Generation of bone marrow chimeras

For bone marrow chimera experiments, recipients were irradiated with 12 Gy and 10^7 donor bone marrow cells were injected intravenously. Mice were given oral antibiotics for 1 week following irradiation. Peripheral blood was analyzed at 8 weeks after transplant for the proportion of donor- and recipient-derived hematopoietic cells based on detection of CD45.1 or CD45.2 isoforms. *Ifnl2*$^{-/-}$*Ifnl3*$^{-/-}$ mice were exclusively maintained as CD45.2. After 8 to 10 weeks of engraftment, chimeric mice were inoculated and analyzed as indicated.

Transmission electron microscopy

For analyses of purified MNoV, samples were fixed with 1% glutaraldehyde (Ted Pella Inc., Redding, CA) and allowed to absorb onto freshly glow-discharged formvar/carbon-coated copper grids for 10 min. Grids were then washed in distilled water and stained with 1% aqueous uranyl acetate (Ted Pella Inc.) for 1 min. Excess liquid was gently wicked off, and grids were allowed to air dry. Samples were viewed on a JEOL 1200EX transmission electron microscope (JEOL USA, Peabody, MA) equipped with an AMT 8-megapixel digital camera (Advanced Microscopy Techniques, Woburn, MA).

For ultrastructural analyses of intestinal tissue, samples were fixed in 2% paraformaldehyde/2.5% glutaraldehyde (Ted Pella Inc., Redding, CA) in 100 mM sodium cacodylate buffer for 2 hours at room temperature and then overnight at 4°C. Samples were washed in sodium cacodylate buffer and postfixed in 1% osmium tetroxide (Ted Pella Inc.) for 1 hour at room temperature. After three washes in distilled water, samples were en bloc stained in 1% aqueous uranyl acetate (Electron Microscopy Sciences, Hatfield, PA) for 1 hour. Samples were then rinsed in distilled water, dehydrated in a graded series of ethanol, and embedded in Eponate 12 resin (Ted Pella Inc.). Ultrathin sections of 95 nm were cut with a Leica Ultracut UCT ultramicrotome (Leica Microsystems Inc., Bannockburn, IL), stained with uranyl acetate and lead citrate, and viewed on a transmission electron microscope as described above.

Quantitative reverse transcription PCR

RNA from stool was isolated using a ZR-96 viral RNA kit (Zymo Research, Irvine, CA). RNA from tissues or cells was isolated using TRI Reagent (Invitrogen) and a Direct-zol-96 RNA kit (Zymo Research, Irvine, CA) according to the manufacturer's protocol. Five microliters of RNA from stool or 1 μg of RNA from tissue was used as a template for cDNA synthesis with the ImPromII reverse transcriptase system (Promega, Madison, WI). DNA contamination was removed using the DNA-free kit (Life Technologies). MNoV TaqMan assays were performed, using a standard curve for determination of absolute viral genome copies, as described previously (*55*). Quantitative polymerase chain reaction (PCR) for housekeeping gene *Rps29* was performed with forward primer 5′-GCAAATACGGGCTGAACATG-3′, reverse primer 5′-GTCCAACTTAATGAAGCCTATGTC-3′, and probe 5′-/5HEX/CCTTCGCGT/ZEN/ACTGCCGGAAGC/3IABkFQ/-3′ (where 3IABkFQ is 3′ Iowa Black fluorescence quencher; Integrated DNA Technologies), each at a concentration of 0.2 μM, using AmpliTaq gold DNA polymerase (Applied Biosystems). Quantitative PCRs for *Ifnlr1* (Mm.PT.58.10781457) and *Mavs* (Mm.PT.58.28896835 and Mm00523169_m1) were similarly performed using PrimeTime qPCR assays (Integrated DNA Technologies).

Isolation of IECs, tuft cells, and goblet cells

Isolation of the epithelial fraction of the intestine was performed as previously described (*17*, *56*). Briefly, mice were euthanized, and intestine was collected in cold PBS. Tissues were washed with cold PBS twice, chopped, and transferred to new tubes followed by incubation in stripping buffer [10% fetal bovine serum (FBS), 15 mM Hepes, 5 mM EDTA, in 1× Hanks' balanced salt solution] for 20 min at 37°C. The tissues were vortexed for 15 s and passed sequentially through 100- and 40-μm filters. The dissociated cells were collected as the epithelial fraction, consisting predominantly of IECs.

For goblet cell sorting (*56*), collected cells were washed with cold PBS and stained with live/dead staining kit (live/dead fixable blue dead cell stain kit, Life Technologies) according to the manufacturer's protocol. After live/dead staining, cells were stained with anti-CD24 (eBioscience; clone 30-F1), anti-CD45 (BioLegend, clone 30-F11), anti–UEA-1 (Vector Laboratories), and anti–cytokeratin 18 (Abcam, clone C-04). Goblet cells were sorted using a BD ARIA II cell sorter (BD Biosciences) by gating on CD45$^-$CD24$^-$CK-18$^+$UEA-1$^+$, while the remaining IECs were collected by gating on CD45$^-$CD24$^-$CK-18$^-$UEA-1$^-$ and collected in RPMI containing 10% FBS. Similarly, for tuft cell sorting, live/dead staining and then staining for anti-SiglecF (BioLegend, clone S17007L) were performed and tuft cells were sorted as CD45$^-$Epcam$^+$SiglecF$^+$. For both sorted goblet and tuft cells, collected cells were centrifuged and resuspended in TRI Reagent (Invitrogen) for RNA extraction. Data were processed using FACSDiva software (BD Biosciences) and FlowJo (BD Biosciences).

RNAscope and histology

The RNAscope Multiplex Fluorescent Detection Kit v2 (Advanced Cell Diagnostics, Newark, CA) was used to perform hybridizations with MNoV probes (Opal 520; Akoya Biosciences) in combination with anti-DCLK1 antibody (Abcam; ab31704) on fixed frozen or paraffin-embedded sections. Tissues were stained with anti-DCLK1 antibody overnight at 4°C and then detected by Alexa Fluor 594–conjugated secondary antibodies (Invitrogen). Tissues were counterstained with DAPI (4′,6-diamidino-2-phenylindole) and mounted using VectaMount mounting medium (Vector Laboratories). Images were acquired using an ApoTome microscope

(Zeiss), and images were captured using Axiovision 4.8.2 software (Zeiss). Images are representative of two independent experiments.

Analysis of single-cell RNAseq data

A previously generated single-cell RNAseq dataset of mouse small intestinal epithelium (*27*) [publicly available at the National Center for Biotechnology Information's (NCBI) Gene Expression Omnibus (GEO), accession #GSE92332] was accessed using the Broad Institute's Single Cell Portal (SCP) (https://singlecell.broadinstitute.org/single_cell). Bubble and tSNE plots of *Cd300lf*, *Vav1*, and *Mavs* expression were generated in SCP.

Supplementary Materials

This PDF file includes:

Figs. S1 to S4

REFERENCES AND NOTES

1. S. M. Pires, C. L. Fischer-Walker, C. F. Lanata, B. Devleesschauwer, A. J. Hall, M. D. Kirk, A. S. R. Duarte, R. E. Black, F. J. Angulo, Aetiology-specific estimates of the global and regional incidence and mortality of diarrhoeal diseases commonly transmitted through food. *PLOS ONE* **10**, e0142927 (2015).
2. J. A. Platts-Mills, S. Babji, L. Bodhidatta, J. Gratz, R. Haque, A. Havt, B. McCormick, M. McGrath, M. P. Olortegui, A. Samie, S. Shakoor, D. Mondal, I. F. Lima, D. Hariraju, B. B. Rayamajhi, S. Qureshi, F. Kabir, P. P. Yori, B. Mufamadi, C. Amour, J. D. Carreon, S. A. Richard, D. Lang, P. Bessong, E. Mduma, T. Ahmed, A. A. Lima, C. J. Mason, A. K. Zaidi, Z. A. Bhutta, M. Kosek, R. L. Guerrant, M. Gottlieb, M. Miller, G. Kang, E. R. Houpt; MAL-ED Network Investigators, Pathogen-specific burdens of community diarrhoea in developing countries: A multisite birth cohort study (MAL-ED). *Lancet Glob. Health* **3**, e564–e575 (2015).
3. B. A. Lopman, D. Steele, C. D. Kirkwood, U. D. Parashar, The vast and varied global burden of norovirus: Prospects for prevention and control. *PLOS Med.* **13**, e1001999 (2016).
4. K. Ettayebi, S. E. Crawford, K. Murakami, J. R. Broughman, U. Karandikar, V. R. Tenge, F. H. Neill, S. E. Blutt, X. L. Zeng, L. Qu, B. Kou, A. R. Opekun, D. Burrin, D. Y. Graham, S. Ramani, R. L. Atmar, M. K. Estes, Replication of human noroviruses in stem cell-derived human enteroids. *Science* **353**, 1387–1393 (2016).
5. S. C. Lin, L. Qu, K. Ettayebi, S. E. Crawford, S. E. Blutt, M. J. Robertson, X. L. Zeng, V. R. Tenge, B. V. Ayyar, U. C. Karandikar, X. Yu, C. Coarfa, R. L. Atmar, S. Ramani, M. K. Estes, Human norovirus exhibits strain-specific sensitivity to host interferon pathways in human intestinal enteroids. *Proc. Natl. Acad. Sci. U.S.A.* **117**, 23782–23793 (2020).
6. K. Y. Green, S. S. Kaufman, B. M. Nagata, N. Chaimongkol, D. Y. Kim, E. A. Levenson, C. M. Tin, A. B. Yardley, J. A. Johnson, A. B. F. Barletta, K. M. Khan, N. A. Yazigi, S. Subramanian, S. R. Moturi, T. M. Fishbein, I. N. Moore, S. V. Sosnovtsev, Human norovirus targets enteroendocrine epithelial cells in the small intestine. *Nat. Commun.* **11**, 2759 (2020).
7. U. C. Karandikar, S. E. Crawford, N. J. Ajami, K. Murakami, B. Kou, K. Ettayebi, G. A. Papanicolaou, U. Jongwutiwes, M. A. Perales, J. Shia, D. Mercer, M. J. Finegold, J. Vinjé, R. L. Atmar, M. K. Estes, Detection of human norovirus in intestinal biopsies from immunocompromised transplant patients. *J. Gen. Virol.* **97**, 2291–2300 (2016).
8. L. B. Thackray, C. E. Wobus, K. A. Chachu, B. Liu, E. R. Alegre, K. S. Henderson, S. T. Kelley, H. W. Virgin IV, Murine noroviruses comprising a single genogroup exhibit biological diversity despite limited sequence divergence. *J. Virol.* **81**, 10460–10473 (2007).
9. T. J. Nice, D. W. Strong, B. T. McCune, C. S. Pohl, H. W. Virgin, A single-amino-acid change in murine norovirus NS1/2 is sufficient for colonic tropism and persistence. *J. Virol.* **87**, 327–334 (2013).
10. V. R. Graziano, M. M. Alfajaro, C. O. Schmitz, R. B. Filler, M. S. Strine, J. Wei, L. L. Hsieh, M. T. Baldridge, T. J. Nice, S. Lee, R. C. Orchard, C. B. Wilen, CD300lf conditional knockout mouse reveals strain-specific cellular tropism for murine norovirus. *J. Virol.* **95**, e01652-20 (2020).
11. V. R. Graziano, F. C. Walker, E. A. Kennedy, J. Wei, K. Ettayebi, M. S. Strine, R. B. Filler, E. Hassan, L. L. Hsieh, A. S. Kim, A. O. Kolawole, C. E. Wobus, L. C. Lindesmith, R. S. Baric, M. K. Estes, R. C. Orchard, M. T. Baldridge, C. B. Wilen, CD300lf is the primary physiologic receptor of murine norovirus but not human norovirus. *PLOS Pathog.* **16**, e1008242 (2020).
12. C. B. Wilen, S. Lee, L. L. Hsieh, R. C. Orchard, C. Desai, B. L. Hykes Jr., M. R. McAllaster, D. R. Balce, T. Feehley, J. R. Brestoff, C. A. Hickey, C. C. Yokoyama, Y. T. Wang, D. A. MacDuff, D. Kreamalmayer, M. R. Howitt, J. A. Neil, K. Cadwell, P. M. Allen, S. A. Handley, M. van Lookeren Campagne, M. T. Baldridge, H. W. Virgin, Tropism for tuft cells determines immune promotion of norovirus pathogenesis. *Science* **360**, 204–208 (2018).
13. M. S. Strine, M. M. Alfajaro, V. R. Graziano, J. Song, L. L. Hsieh, R. Hill, J. Guo, K. L. VanDussen, R. C. Orchard, M. T. Baldridge, S. Lee, C. B. Wilen, Tuft-cell-intrinsic and -extrinsic mediators of norovirus tropism regulate viral immunity. *Cell Rep.* **41**, 111593 (2022).
14. J. von Moltke, M. Ji, H. E. Liang, R. M. Locksley, Tuft-cell-derived IL-25 regulates an intestinal ILC2-epithelial response circuit. *Nature* **529**, 221–225 (2016).
15. F. Gerbe, E. Sidot, D. J. Smyth, M. Ohmoto, I. Matsumoto, V. Dardalhon, P. Cesses, L. Garnier, M. Pouzolles, B. Brulin, M. Bruschi, Y. Harcus, V. S. Zimmermann, N. Taylor, R. M. Maizels, P. Jay, Intestinal epithelial tuft cells initiate type 2 mucosal immunity to helminth parasites. *Nature* **529**, 226–230 (2016).
16. M. R. Howitt, S. Lavoie, M. Michaud, A. M. Blum, S. V. Tran, J. V. Weinstock, C. A. Gallini, K. Redding, R. F. Margolskee, L. C. Osborne, D. Artis, W. S. Garrett, Tuft cells, taste-chemosensory cells, orchestrate parasite type 2 immunity in the gut. *Science* **351**, 1329–1333 (2016).
17. M. T. Baldridge, S. Lee, J. J. Brown, N. McAllister, K. Urbanek, T. S. Dermody, T. J. Nice, H. W. Virgin, Expression of *Ifnlr1* on intestinal epithelial cells is critical to the antiviral effects of interferon lambda against norovirus and reovirus. *J. Virol.* **91**, e02079-16 (2017).
18. T. J. Nice, M. T. Baldridge, B. T. McCune, J. M. Norman, H. M. Lazear, M. Artyomov, M. S. Diamond, H. W. Virgin, Interferon-λ cures persistent murine norovirus infection in the absence of adaptive immunity. *Science* **347**, 269–273 (2015).
19. J. A. Van Winkle, S. T. Peterson, E. A. Kennedy, M. J. Wheadon, H. Ingle, C. Desai, R. Rodgers, D. A. Constant, A. P. Wright, L. Li, M. N. Artyomov, S. Lee, M. T. Baldridge, T. J. Nice, Homeostatic interferon-lambda response to bacterial microbiota stimulates preemptive antiviral defense within discrete pockets of intestinal epithelium. *eLife* **11**, e74072 (2022).
20. S. A. McCartney, L. B. Thackray, L. Gitlin, S. Gilfillan, H. W. Virgin IV, M. Colonna, MDA-5 recognition of a murine norovirus. *PLOS Pathog.* **4**, e1000108 (2008).
21. D. A. MacDuff, M. T. Baldridge, A. M. Qaqish, T. J. Nice, A. D. Darbandi, V. L. Hartley, S. T. Peterson, J. J. Miner, K. Iwai, H. W. Virgin, HOIL1 is essential for the induction of type I and III interferons by MDA5 and regulates persistent murine norovirus infection. *J. Virol.* **92**, e01368-18 (2018).
22. S. Lee, C. B. Wilen, A. Orvedahl, B. T. McCune, K. W. Kim, R. C. Orchard, S. T. Peterson, T. J. Nice, M. T. Baldridge, H. W. Virgin, Norovirus cell tropism is determined by combinatorial action of a viral non-structural protein and host cytokine. *Cell Host Microbe* **22**, 449–459.e4 (2017).
23. S. T. Peterson, E. A. Kennedy, P. H. Brigleb, G. M. Taylor, K. Urbanek, T. L. Bricker, S. Lee, H. Shin, T. S. Dermody, A. C. M. Boon, M. T. Baldridge, Disruption of type III interferon (IFN) genes *Ifnl2* and *Ifnl3* recapitulates loss of the type III IFN receptor in the mucosal antiviral response. *J. Virol.* **93**, e01073-19 (2019).
24. K. Roe, D. Giordano, L. B. Young, K. E. Draves, U. Holder, M. S. Suthar, M. Gale, E. A. Clark, Dendritic cell-associated MAVS is required to control West Nile virus replication and ensuing humoral immune responses. *PLOS ONE* **14**, e0218928 (2019).
25. P. B. Stranges, J. Watson, C. J. Cooper, C. M. Choisy-Rossi, A. C. Stonebraker, R. A. Beighton, H. Hartig, J. P. Sundberg, S. Servick, G. Kaufmann, P. J. Fink, A. V. Chervonsky, Elimination of antigen-presenting cells and autoreactive T cells by Fas contributes to prevention of autoimmunity. *Immunity* **26**, 629–641 (2007).
26. B. B. Madison, L. Dunbar, X. T. Qiao, K. Braunstein, E. Braunstein, D. L. Gumucio, Cis elements of the villin gene control expression in restricted domains of the vertical (crypt) and horizontal (duodenum, cecum) axes of the intestine. *J. Biol. Chem.* **277**, 33275–33283 (2002).
27. A. L. Haber, M. Biton, N. Rogel, R. H. Herbst, K. Shekhar, C. Smillie, G. Burgin, T. M. Delorey, M. R. Howitt, Y. Katz, I. Tirosh, S. Beyaz, D. Dionne, M. Zhang, R. Raychowdhury, W. S. Garrett, O. Rozenblatt-Rosen, H. N. Shi, O. Yilmaz, R. J. Xavier, A. Regev, A single-cell survey of the small intestinal epithelium. *Nature* **551**, 333–339 (2017).
28. M. S. Nadjsombati, J. W. McGinty, M. R. Lyons-Cohen, J. B. Jaffe, L. DiPeso, C. Schneider, C. N. Miller, J. L. Pollack, G. A. Nagana Gowda, M. F. Fontana, D. J. Erle, M. S. Anderson, R. M. Locksley, D. Raftery, J. von Moltke, Detection of succinate by intestinal tuft cells triggers a type 2 innate immune circuit. *Immunity* **49**, 33–41.e7 (2018).
29. V. Matei, S. Pauley, S. Kaing, D. Rowitch, K. W. Beisel, K. Morris, F. Feng, K. Jones, J. Lee, B. Fritzsch, Smaller inner ear sensory epithelia in Neurog 1 null mice are related to earlier hair cell cycle exit. *Dev. Dyn.* **234**, 633–650 (2005).
30. P. W. Tetteh, O. Basak, H. F. Farin, K. Wiebrands, K. Kretzschmar, H. Begthel, M. van den Born, J. Korving, F. de Sauvage, J. H. van Es, A. van Oudenaarden, H. Clevers, Replacement of lost Lgr5-positive stem cells through plasticity of their enterocyte-lineage daughters. *Cell Stem Cell* **18**, 203–213 (2016).
31. N. F. Shroyer, M. A. Helmrath, V. Y.–. C. Wang, B. Antalffy, S. J. Henning, H. Y. Zoghbi, Intestine-specific ablation of mouse atonal homolog 1 (Math1) reveals a role in cellular homeostasis. *Gastroenterology* **132**, 2478–2488 (2007).

32. F. Gerbe, J. H. van Es, L. Makrini, B. Brulin, G. Mellitzer, S. Robine, B. Romagnolo, N. F. Shroyer, J. F. Bourgaux, C. Pignodel, H. Clevers, P. Jay, Distinct ATOH1 and Neurog3 requirements define tuft cells as a new secretory cell type in the intestinal epithelium. *J. Cell Biol.* **192**, 767–780 (2011).
33. S. M. Karst, C. E. Wobus, M. Lay, J. Davidson, H. W. T. Virgin, STAT1-dependent innate immunity to a Norwalk-like virus. *Science* **299**, 1575–1578 (2003).
34. M. B. Uccellini, A. Garcia-Sastre, ISRE-reporter mouse reveals high basal and induced type I IFN responses in inflammatory monocytes. *Cell Rep.* **25**, 2784–2796.e3 (2018).
35. Y. Du, H. Gao, C. He, S. Xin, B. Wang, S. Zhang, F. Gong, X. Yu, L. Pan, F. Sun, W. Wang, J. Xu, An update on the biological characteristics and functions of tuft cells in the gut. *Front. Cell Dev. Biol.* **10**, 1102978 (2022).
36. Y. Nakanishi, H. Seno, A. Fukuoka, T. Ueo, Y. Yamaga, T. Maruno, N. Nakanishi, K. Kanda, H. Komekado, M. Kawada, A. Isomura, K. Kawada, Y. Sakai, M. Yanagita, R. Kageyama, Y. Kawaguchi, M. M. Taketo, S. Yonehara, T. Chiba, Dclk1 distinguishes between tumor and normal stem cells in the intestine. *Nat. Genet.* **45**, 98–103 (2013).
37. C. B. Westphalen, S. Asfaha, Y. Hayakawa, Y. Takemoto, D. J. Lukin, A. H. Nuber, A. Brandtner, W. Setlik, H. Remotti, A. Muley, X. Chen, R. May, C. W. Houchen, J. G. Fox, M. D. Gershon, M. Quante, T. C. Wang, Long-lived intestinal tuft cells serve as colon cancer-initiating cells. *J. Clin. Invest.* **124**, 1283–1295 (2014).
38. M. Santiana, S. Ghosh, B. A. Ho, V. Rajasekaran, W. L. du, Y. Mutsafi, D. A. de Jésus-Diaz, S. V. Sosnovtsev, E. A. Levenson, G. I. Parra, P. M. Takvorian, A. Cali, C. Bleck, A. N. Vlasova, L. J. Saif, J. T. Patton, P. Lopalco, A. Corcelli, K. Y. Green, N. Altan-Bonnet, Vesicle-cloaked virus clusters are optimal units for inter-organismal viral transmission. *Cell Host Microbe* **24**, 208–220.e8 (2018).
39. J. M. Devant, G. S. Hansman, Structural heterogeneity of a human norovirus vaccine candidate. *Virology* **553**, 23–34 (2021).
40. M. B. Sherman, A. N. Williams, H. Q. Smith, C. Nelson, C. B. Wilen, D. H. Fremont, H. W. Virgin, T. J. Smith, Bile salts alter the mouse norovirus capsid conformation: Possible implications for cell attachment and immune evasion. *J. Virol.* **93**, e00970-19 (2019).
41. C. A. Nelson, C. B. Wilen, Y. N. Dai, R. C. Orchard, A. S. Kim, R. A. Stegeman, L. L. Hsieh, T. J. Smith, H. W. Virgin, D. H. Fremont, Structural basis for murine norovirus engagement of bile acids and the CD300lf receptor. *Proc. Natl. Acad. Sci. U.S.A.* **115**, E9201–E9210 (2018).
42. M. B. Sherman, A. N. Williams, H. Q. Smith, B. M. Pettitt, C. E. Wobus, T. J. Smith, Structural studies on the shapeshifting murine norovirus. *Viruses* **13**, 2162 (2021).
43. F. C. Walker, E. Hassan, S. T. Peterson, R. Rodgers, L. A. Schriefer, C. E. Thompson, Y. Li, G. Kalugotla, C. Blum-Johnston, D. Lawrence, B. T. McCune, V. R. Graziano, L. Lushniak, S. Lee, A. N. Roth, S. M. Karst, T. J. Nice, J. J. Miner, C. B. Wilen, M. T. Baldridge, Norovirus evolution in immunodeficient mice reveals potentiated pathogenicity via a single nucleotide change in the viral capsid. *PLOS Pathog.* **17**, e1009402 (2021).
44. Q. Feng, S. V. Hato, M. A. Langereis, J. Zoll, R. Virgen-Slane, A. Peisley, S. Hur, B. L. Semler, R. P. van Rij, F. J. M. van Kuppeveld, MDA5 detects the double-stranded RNA replicative form in picornavirus-infected cells. *Cell Rep.* **2**, 1187–1196 (2012).
45. C. A. Kasper, I. Sorg, C. Schmutz, T. Tschon, H. Wischnewski, M. L. Kim, C. Arrieumerlou, Cell-cell propagation of NF-κB transcription factor and MAP kinase activation amplifies innate immunity against bacterial infection. *Immunity* **33**, 804–816 (2010).
46. A. Ablasser, J. L. Schmid-Burgk, I. Hemmerling, G. L. Horvath, T. Schmidt, E. Latz, V. Hornung, Cell intrinsic immunity spreads to bystander cells via the intercellular transfer of cGAMP. *Nature* **503**, 530–534 (2013).
47. B. Hoover, V. Baena, M. M. Kaelberer, F. Getaneh, S. Chinchilla, D. V. Bohórquez, The intestinal tuft cell nanostructure in 3D. *Sci. Rep.* **7**, 1652 (2017).
48. Y. Fu, R. Zi, S. Xiong, Infection by exosome-carried Coxsackievirus B3 induces immune escape resulting in an aggravated pathogenesis. *Microbes Infect.* **105148**, (2023).
49. E. A. Kennedy, S. Aggarwal, A. Dhar, S. M. Karst, C. B. Wilen, M. T. Baldridge, Age-associated features of norovirus infection analysed in mice. *Nat. Microbiol.* **8**, 1095–1107 (2023).
50. A. Janowska-Wieczorek, M. Majka, J. Kijowski, M. Baj-Krzyworzeka, R. Reca, A. R. Turner, J. Ratajczak, S. G. Emerson, M. A. Kowalska, M. Z. Ratajczak, Platelet-derived microparticles bind to hematopoietic stem/progenitor cells and enhance their engraftment. *Blood* **98**, 3143–3149 (2001).
51. J. de Boer, A. Williams, G. Skavdis, N. Harker, M. Coles, M. Tolaini, T. Norton, K. Williams, K. Roderick, A. . J. Potocnik, D. Kioussis, Transgenic mice with hematopoietic and lymphoid specific expression of Cre. *Eur. J. Immunol.* **33**, 314–325 (2003).
52. S. Srinivas, T. Watanabe, C. S. Lin, C. M. William, Y. Tanabe, T. M. Jessell, F. Costantini, Cre reporter strains produced by targeted insertion of EYFP and ECFP into the ROSA26 locus. *BMC Dev. Biol.* **1**, 4 (2001).
53. D. W. Strong, L. B. Thackray, T. J. Smith, H. W. Virgin, Protruding domain of capsid protein is necessary and sufficient to determine murine norovirus replication and pathogenesis in vivo. *J. Virol.* **86**, 2950–2958 (2012).
54. R. C. Orchard, C. B. Wilen, J. G. Doench, M. T. Baldridge, B. T. McCune, Y.-C. J. Lee, S. Lee, S. M. Pruett-Miller, C. A. Nelson, D. H. Fremont, H. W. Virgin, Discovery of a proteinaceous cellular receptor for a norovirus. *Science* **353**, 933–936 (2016).
55. L. Baert, C. E. Wobus, E. van Coillie, L. B. Thackray, J. Debevere, M. Uyttendaele, Detection of murine norovirus 1 by using plaque assay, transfection assay, and real-time reverse transcription-PCR before and after heat exposure. *Appl. Environ. Microbiol.* **74**, 543–546 (2008).
56. H. Ingle, E. Hassan, J. Gawron, B. Mihi, Y. Li, E. A. Kennedy, G. Kalugotla, H. Makimaa, S. Lee, P. Desai, K. G. McDonald, M. S. Diamond, R. D. Newberry, M. Good, M. T. Baldridge, Murine astrovirus tropism for goblet cells and enterocytes facilitates an IFN-λ response in vivo and in enteroid cultures. *Mucosal Immunol.* **14**, 751–761 (2021).

Acknowledgments: We thank all members of the Baldridge laboratory for helpful discussions. We also acknowledge W. Beatty of the Washington Molecular Microbiology Imaging Facility for assistance with electron microscopy. We additionally thank H. Clevers and O. Yilmaz for provision of *Alpi-Cre^{ERT2}* mice and T. Wang for providing *Dclk1cre* mice. **Funding:** This work was supported by NIH grants R01AI127552, R01AI139314, and R01AI141478; The G. Harold and Leila Y. Mathers Foundation; and the Pew Biomedical Scholars Program of the Pew Charitable Trusts (M.T.B.). H.M. was supported by NIH grant R25GM103757. E.A.K. was supported by NSF grant DGE-1745038/DGE-2139839 and NIH grant F31AI167499. S.L. was supported by R00 AI141683, P20 GM109035, the Smith Family Foundation, and the Charles H. Hood Foundation. The Washington University Center for Cellular Imaging (WUCCI) is supported by the Office of Research Infrastructure Programs (ORIP), a part of the NIH Office of the Director under grant OD030233. **Author contributions:** H.I., H.M., S.A., H.D., L.F., Y.L., E.A.K., and S.T.P. performed the experiments. H.I. and M.T.B. analyzed the results. H.I., C.B.W., S.L., and M.T.B. designed the project. M.S.S. provided critical mouse resources. H.I. and M.T.B. wrote the manuscript. All authors read and edited the manuscript. **Competing interests:** The authors declare that they have no competing interests. **Data and materials availability:** All data needed to evaluate the conclusions in the paper are present in the paper and/or the Supplementary Materials. Mouse lines and viral stocks can be provided by Dr. Baldridge at Washington University School of Medicine pending scientific review and a completed material transfer agreement. Requests for these materials should be submitted to: mbaldridge@wustl.edu.

Submitted 13 April 2023
Accepted 10 August 2023
Published 13 September 2023
10.1126/sciadv.adi2562